JOURNAL OF Applied Polymer SCIENCE

Synthesis and Gas Transport Properties of Novel Hyperbranched Polyimide–Silica Hybrid Membranes

Tomoyuki Suzuki, Yasuharu Yamada
Department of Biomolecular Engineering, Kyoto Institute of Technology, Matsugasaki, Sakyo-ku, Kyoto 606-8585, Japan
Correspondence to: Y. Yamada (E-mail: y-yamada@kit.ac.jp)

ABSTRACT: Physical and gas transport properties of hyperbranched polyimide (HBPI)—silica hybrid membranes prepared with a dianhydride monomer, 4,4′-(hexafluoroisopropylidene)diphthalic anhydride (6FDA), and triamine monomers, 1,3,5-tris(4-aminophenoxy)triazine (TAPOTZ), and 1,3,5-tris(4-aminophenyl)benzene (TAPB), were investigated and compared with those of 6FDA-TAPOB HBPI system synthesized from 6FDA and 1,3,5-tris(4-aminophenoxy)benzene (TAPOB). Glass transition and 5% weight-loss temperatures of the 6FDA-based HBPI–silica hybrid membranes were increased with increasing silica content. 6FDA-TAPOTZ HBPI system, however, showed relatively low 5% weight-loss temperatures, suggesting thermal instability of triazine-ring in the TAPOTZ moiety. CO_2/CH_4 permselectivity of the HBPI–silica hybrid membranes were increased with increasing silica content, tending to exceed the upper bound for CO_2/CH_4 separation. This result indicated that free volume elements effective for CO_2/CH_4 separation were created by the incorporation of silica for the HBPI–silica hybrid systems. Especially, 6FDA-TAPB HBPI system had high gas permeabilities and CO_2/CH_4 separation ability, arising from high fractional free volume and characteristic size and distribution of free volume elements. © 2012 Wiley Periodicals, Inc. J. Appl. Polym. Sci. 000: 000–000, 2012

KEYWORDS: hyperbranched polyimide; silica hybrid; sol–gel, gas permeation; gas separation

Received 23 January 2012; accepted 13 April 2012; published online
DOI: 10.1002/app.37893

INTRODUCTION

Gas separation processes using polymeric membranes have greatly been developed during the last few decades. Especially, polyimides have attracted much attention as gas separation membranes because of their high gas permselectivities and excellent thermal and mechanical properties.[1–4] In recent years, hyperbranched polyimides (HBPIs) have been synthesized and characterized. The HBPIs have different gas transport properties from linear-type polyimides, and are extensively expected as high-performance gas separation materials.[5–7] In our previous study, gas transport properties of the HBPI prepared by polycondensation of a dianhydride, 4,4′-(hexafluoroisopropylidene)-diphthalic anhydride (6FDA) and a triamine, 1,3,5-tris(4-aminophenoxy)benzene (TAPOB), (HBPI(6FDA-TAPOB)) have been investigated, and it has been found that the HBPI(6FDA-TAPOB) exhibits noticable gas permselectivities arising from a characteristic hyperbranched structure.[8]

Organic–inorganic hybrids are recognized as a new class of advanced materials as they generally possess desirable organic and inorganic properties. Hybridization with inorganic compounds has been focused on the modification of polyimides to improve their thermal, mechanical, and gas transport properties.[9–11] We have also reported that gas permeabilities and CO_2/CH_4 separation capability of HBPI–silica hybrid membranes prepared with commercially available dianhydride monomers and TAPOB are significantly increased with increasing silica content, suggesting characteristic distribution, and interconnectivity of free volume elements created by the incorporation of silica.[12,13]

In this study, physical and gas transport properties of novel HBPIs prepared with 6FDA as a dianhydride monomer and triamine monomers, 1,3,5-tris(4-aminophenoxy)triazine (TAPOTZ) and 1,3,5-tris(4-aminophenyl)benzene (TAPB), and their silica hybrids were investigated. In addition, obtained physical and gas transport properties of the HBPI(6FDA-TAPOTZ) and HBPI(6FDA-TAPB) systems are compared with those of the HBPI(6FDA-TAPOB) system reported previously.[14]

EXPERIMENTAL

Materials

TAPOB was synthesized by reduction of 1,3,5-tris(4-nitrophenoxy)benzene with palladium carbon and hydrazine in methanol.[15]

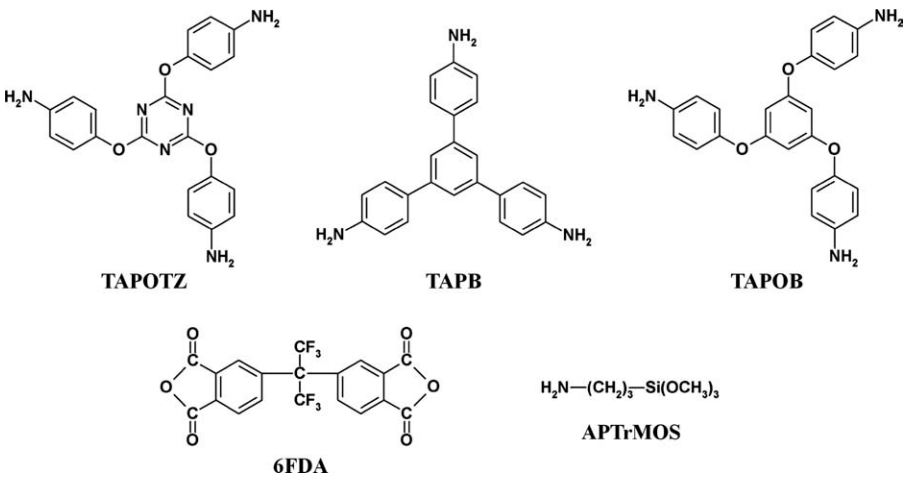

Figure 1. Chemical structures of monomers.

Dianhydride monomer, 6FDA, and triamine monomers, TAPOTZ and TAPB, were kindly supplied from Daikin Industries (Osaka, Japan) and Wakayama Seika Kogyo Co. (Wakayama, Japan), respectively. 3-aminopropyltrimethoxysilane (APTrMOS) and tetramethoxysilane (TMOS) were obtained from AZmax Co., (Tokyo, Japan). *N, N*-dimethylacetamide (DMAc) as a solvent was purchased from Nacalai Tesque, (Kyoto, Japan). Chemical structures of monomers are shown in Figure 1.

Polymerization

Three millimoles of 6FDA was dissolved in 40 mL of DMAc in a 100-mL three-neck flask under N_2 flow at room temperature. To this solution, 1.6 mmol of triamine (TAPOTZ or TAPB) in 20 mL of DMAc was added dropwise through a syringe with stirring for 3 h. After that 0.4 mmol of APTrMOS as a coupling agent was added in the reaction mixture with stirring for 1 h to afford hyperbranched polyamic acid.

Membrane formation

The HBPI–silica hybrid membranes were prepared by thermal imidization and sol-gel reaction with alkoxysilane, TMOS. Appropriate amounts of TMOS and deionized water (TMOS: deionized water = 1:6 as a molar ratio) were added in the DMAc solutions of the hyperbranched polyamic acids. The mixed solutions were stirred for 24 h and cast on PET sheets and dried at 85°C for 3 h in a heating oven to form thin membranes. The prepared membranes were peeled off and subsequently imidized and hybridized at 100°C for 1 h, 200°C for 1 h, and 300°C for 1 h in a heating oven under N_2 flow. Finally, HBPI(6FDA-TAPOTZ)—and HBPI(6FDA-TAPB)—silica hybrid membranes (thickness range; 20–25 μm) were successfully prepared.

Measurements

Attenuated total reflection Fourier transform infrared (ATR FT-IR) spectra were recorded at a wavenumber range of 550–4000 cm^{-1} and a resolution of 1 cm^{-1} with a JASCO FT/IR-460 plus. Scanning electron microscopy (SEM) images were acquired using a Hitachi S-3400N variable pressure SEM at an accelerating voltage of 15 kV. Samples for SEM analysis were coated using a Hitachi E-1010 ion sputter coater with a platinum target. UV/VIS optical transmittances were investigated by a JASCO V-530 UV/VIS spectrometer at a wavelength of 200–800 nm. Thermogravimetric-differential thermal analysis (TG-DTA) experiments were performed with a Seiko TG/DTA6300 at a heating rate of 10°C/min under air flow and in the temperature range of 25–800°C. Thermal mechanical analysis (TMA) measurements were undergone using a Seiko TMA/SS6100 at a heating rate of 5°C/min under N_2 flow. CO_2, O_2, N_2, and CH_4 permeation measurements were carried out by a constant volume/variable pressure apparatus at 76 cm Hg and 25°C. The permeability coefficient, P (cm^3(STP)cm/cm^2 s cm Hg), was determined by the following equation;[16]

$$P = \frac{273}{T} \cdot \frac{V}{A} \cdot L \cdot \frac{1}{p} \cdot \frac{1}{76} \cdot \frac{dp}{dt} \tag{1}$$

where T is the absolute temperature (K), V is the downstream volume (cm^3), A is the membrane area (cm^2), L is the membrane

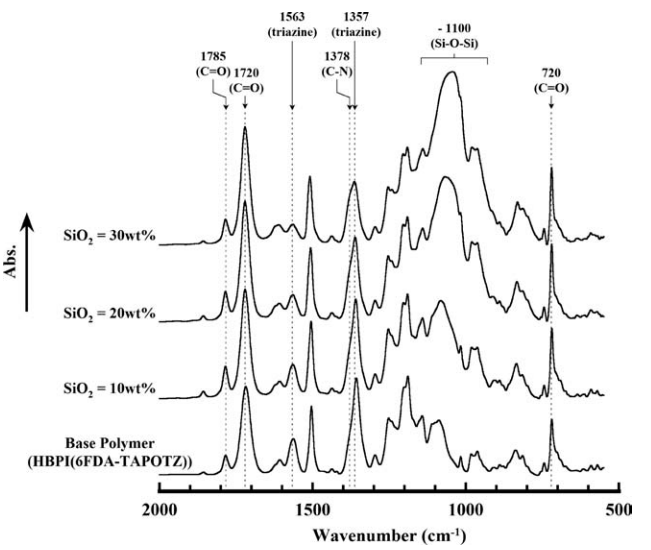

Figure 2. ATR FT-IR spectra of HBPI(6FDA-TAPOTZ)–silica hybrid membranes.

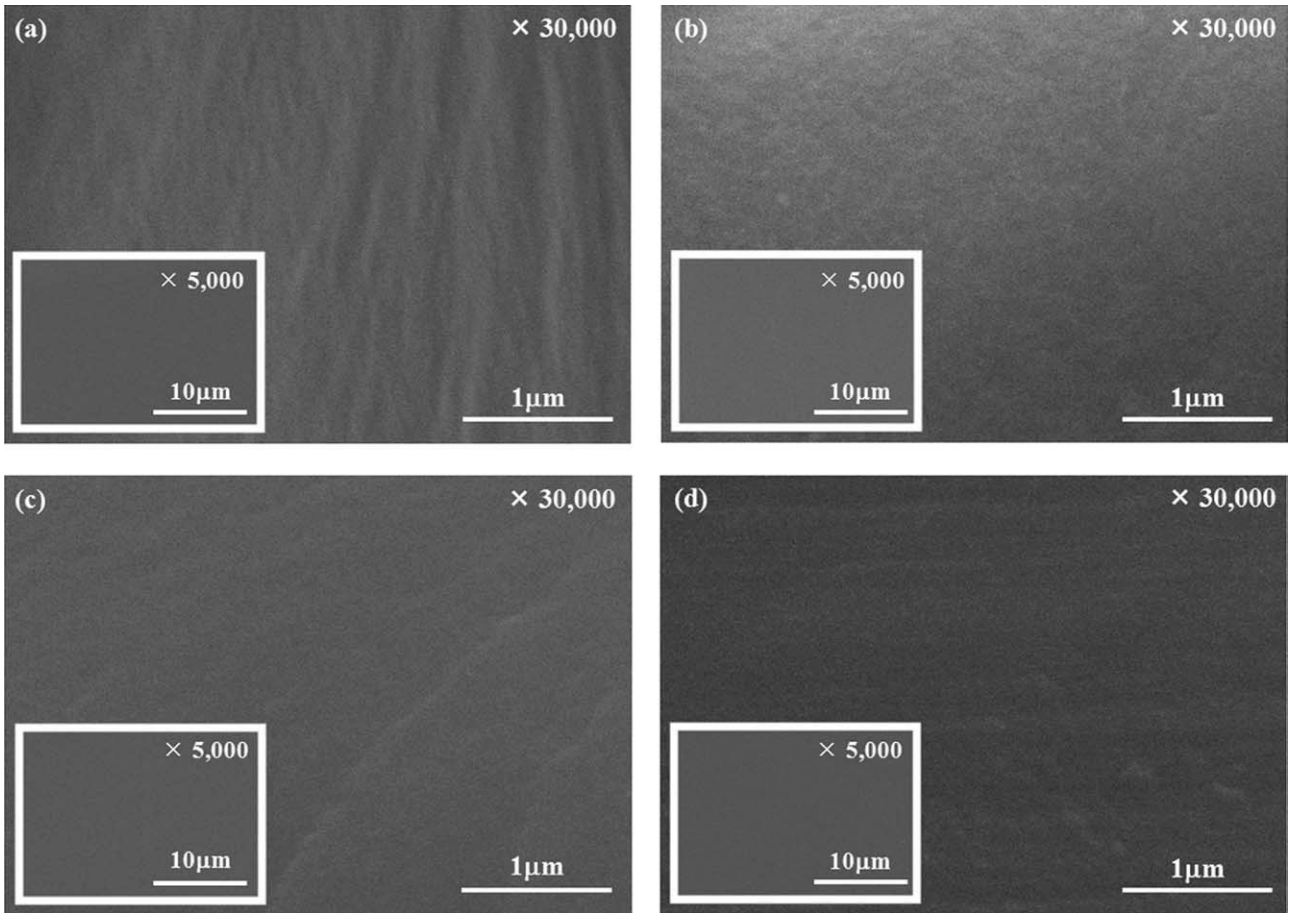

Figure 3. Cross-sectional SEM images of HBPI(6FDA-TAPOB)–silica hybrid membranes; silica content = 0 (a), 10 (b), 20 (c), and 30 wt % (d). Small windows represent surface SEM images of the membranes.

thickness (cm), p is the upstream pressure (cm Hg), and dp/dt is the permeation rate (cm Hg/s). The obtained permeability coefficient contains the error of ~±5% associated with the dispersion of the membrane thickness. The gas permeability coefficient can be explained on the basis of the solution-diffusion mechanism, which is represented by the following equation;

$$P = D \times S \tag{2}$$

Table I. Physical Properties of HBPI–Silica Hybrid Membranes

Sample	Transmittance[a] (%)	T_g[b] (°C)	T_d^{5c}[c] (°C)	Silica content[d] (wt %)	CTE[e] (ppm/°C)	FFV
HBPI(6FDA-TAPOTZ)	85.4	278	406	0	48	0.148
10 wt % SiO_2	89.7	286	450	8	38	-
20 wt % SiO_2	90.3	n.d.[f]	468	21	-	-
30 wt % SiO_2	92.6	n.d.[f]	471	31	-	-
HBPI(6FDA-TAPB)	87.2	324	482	0	49	0.172
10 wt % SiO_2	88.0	n.d.[f]	497	9	44	-
20 wt % SiO_2	88.8	n.d.[f]	498	18	32	-
30 wt % SiO_2	88.8	n.d.[f]	502	30	24	-
HBPI(6FDA-TAPOB)	88.9	282	457	0	54	0.165
10 wt % SiO_2	89.9	305	490	10	47	-
20 wt % SiO_2	90.2	311	496	20	38	-
30 wt % SiO_2	90.3	318	509	30	31	-

[a]Optical transmittance at 600 nm, [b]Glass transition temperature determined by the TG-DTA measurement, [c]5 wt % weight-loss temperature, [d]SiO_2 content determined from the residual at 800°C, [e]Coefficient of thermal expansion at 100–150°C, [f]Not detected.

Table II. Gas Transport Properties of HBPI–Silica Hybrid Membranes at 25°C and 76 cm Hg

	$P \times 10^{10}$ (cm^3(STP) cm/cm^2 s cm Hg)				D × 10^8 (cm^2/s)				$S \times 10^2$ (cm^3(STP)/$cm^3_{polym.}$cm Hg)			
Sample	CO_2	O_2	N_2	CH_4	CO_2	O_2	N_2	CH_4	CO_2	O_2	N_2	CH_4
HBPI(6FDA-TAPOTZ)	5.1	1.1	0.15	0.072	0.19	0.82	0.17	0.023	27	1.3	0.92	3.1
10 wt % SiO_2	6.9	1.5	0.20	0.091	0.26	1.2	0.20	0.025	27	1.3	0.99	3.5
20 wt % SiO_2	8.4	1.7	0.24	0.093	0.25	1.0	0.19	0.022	34	1.7	1.2	4.2
HBPI(6FDA-TAPB)	25	4.6	0.79	0.44	0.76	2.8	0.57	0.091	33	1.7	1.4	4.8
10 wt % SiO_2	28	4.9	0.87	0.45	0.80	2.5	0.52	0.064	35	2.0	1.7	7.0
20 wt % SiO_2	31	5.0	0.85	0.43	0.75	2.4	0.48	0.052	41	2.1	1.8	8.2
30 wt % SiO_2	47	7.0	1.2	0.55	1.1	3.1	0.64	0.074	44	2.2	1.9	7.4
HBPI(6FDA-TAPOB)	7.4	1.5	0.23	0.098	0.30	1.4	0.25	0.028	25	1.1	0.92	3.5
10 wt % SiO_2	10	2.0	0.31	0.13	0.35	1.5	0.29	0.026	30	1.4	1.1	5.0
20 wt % SiO_2	13	2.1	0.32	0.16	0.37	1.3	0.25	0.030	35	1.7	1.3	5.2
30 wt % SiO_2	23	3.0	0.46	0.24	0.57	1.7	0.29	0.040	41	1.8	1.6	6.0

where D (cm^2/s) is the diffusion coefficient and S (cm^3(STP)/$cm^3_{polym.}$cm Hg) is the solubility coefficient. The diffusion coefficient was calculated by the time-lag method;

$$D = \frac{L^2}{6\theta} \tag{3}$$

where θ (s) is the time-lag. Densities of the pristine HBPIs were measured by floating method with NaBr aqueous solution at 25°C. According to the group contribution method, fractional free volume (FFV) of a polymer can be estimated by the following equations;[17]

$$FFV = \frac{V_{sp} - 1.3V_w}{V_{sp}} \tag{4}$$

$$V_{sp} = \frac{1}{\rho} \tag{5}$$

where V_{sp} (cm^3/mol) is the specific molar volume, V_w (cm^3/mol) is the van der Waals volume of the repeat unit, and ρ (g/cm^3) is the experimental density.

RESULTS AND DISCUSSION

Polymer Characterization

Figure 2 shows ATR FT-IR spectra of the HBPI(6FDA-TAPOTZ)—silica hybrid membranes. The bands observed around 1785 cm^{-1} (C=O asymmetrical stretching), 1720 cm^{-1} (C=O symmetrical stretching), 1378 cm^{-1} (C—N stretching), and 720 cm^{-1} (C=O bending) are characteristic absorption bands of polyimides.[6,18] In contrast, the characteristic band of polyamic acids around 1680 cm^{-1} is not found. These results indicate that the prepared membranes are well imidized. It is also found that the band observed around 1100 cm^{-1} assigned to Si—O—Si stretching increases with increasing silica content,[19,20] indicating sufficient formation of a three-dimensional Si—O—Si network. Similar spectra are observed for the HBPI(6FDA-TAPB) systems (data not shown). In addition, for the HBPI(6FDA-TAPOTZ) system, the bands assigned to triazine ring of TAPOTZ moiety are also observed around 1357 and 1563 cm^{-1}.[21]

Figure 3 shows SEM images of HBPI(6FDA-TAPOB)–silica hybrid membranes. The hybrid membranes have smooth cross-sectional and surface morphologies without aggregated silica domains. Optical transmittances of the HBPI–silica hybrid

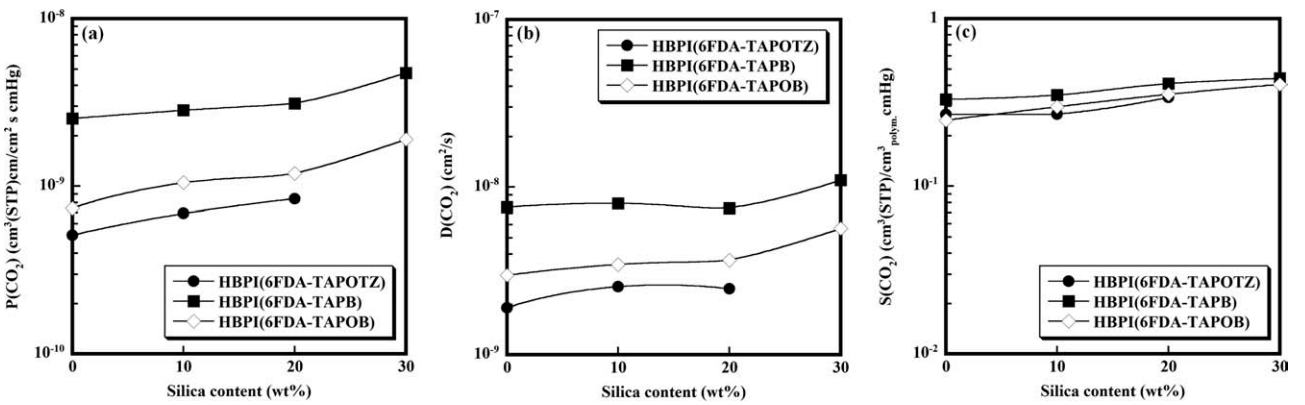

Figure 4. CO_2 permeability (a), diffusion (b), and solubility (c) coefficients of HBPI–silica hybrid membranes plotted against silica content.

Table III. O_2/N_2 and CO_2/CH_4 Selectivities of HBPI–Silica Hybrid Membranes at 25°C and 76 cm Hg

	O_2/N_2 selectivity			CO_2/CH_4 selectivity		
Sample	$\alpha(O_2/N_2)$	$\alpha^D(O_2/N_2)$	$\alpha^S(O_2/N_2)$	$\alpha(CO_2/CH_4)$	$\alpha^D(CO_2/CH_4)$	$\alpha^S(CO_2/CH_4)$
HBPI(6FDA-TAPOTZ)	7.2	4.9	1.5	71	8.4	8.5
10 wt % SiO_2	7.3	5.7	1.3	76	9.9	7.7
20 wt % SiO_2	7.2	5.3	1.4	91	11	8.0
HBPI(6FDA-TAPB)	5.8	4.9	1.2	58	8.3	7.0
10 wt % SiO_2	5.7	4.8	1.2	64	13	5.1
20 wt % SiO_2	5.9	4.9	1.2	73	14	5.0
30 wt % SiO_2	5.7	4.9	1.2	87	15	6.0
HBPI(6FDA-TAPOB)	6.8	5.8	1.2	75	11	7.0
10 wt % SiO_2	6.6	5.2	1.3	79	13	5.9
20 wt % SiO_2	6.7	5.3	1.3	82	12	6.8
30 wt % SiO_2	6.6	5.8	1.1	95	14	6.7

membranes are shown in Table I. The hybrid membranes maintain high transparency similar to corresponding pristine HBPIs. It is also pointed out that the optical transmittances slightly increase with increasing silica content, which might be attributed to decreased imide group density in a unit volume. These facts indicate the HBPI–silica hybrid membranes have high homogeneity, and silica domains are finely dispersed in the HBPIs. The high homogeneity is considered to be brought not only by APTrMOS moiety, which functions as a covalent bond part between organic and inorganic components but also by the characteristic hyperbranched structures of molecular chains.

Thermal properties of the hybrid membranes were investigated by TG-DTA and TMA measurements. Glass transition temperatures (T_gs) determined from DTA curves and 5% weight-loss temperatures (T_d^5s) of the hybrid membranes are summarized in Table I in addition to the residuals at 800°C. It is confirmed from the residuals that all hybrid membranes contain appropriate amounts of silica as expected. T_g values of the hybrid membranes increase with increasing silica content, suggesting the formation of robust three-dimensional Si—O—Si network. However, for the HBPI(6FDA-TAPB) system, T_gs of the hybrid membranes cannot be detected from the DTA curves. This behavior might be attributed to rigid molecular structure of HBPI(6FDA-TAPB) and increased restriction of molecular mobility by hybridization with silica. T_d^5 values of the hybrid membranes are also increased with increasing silica content (Table I). This result indicates the increase in thermal stability of the HBPIs by hybridization with silica. From the comparison of T_d^5 values, HBPI(6FDA-TAPOTZ) system shows lower T_d^5 values than other HBPI systems. The lower T_d^5 values are considered to be due to thermal instability of triazine-ring in the TAPOTZ moiety. Coefficients of thermal expansion (CTEs) from 100 to 150°C of the hybrid membranes are listed in Table I. CTEs of the hybrid membranes are greatly decreased with increasing silica content. This fact means the enhancement of thermal mechanical stability of the HBPIs by hybridization with silica.

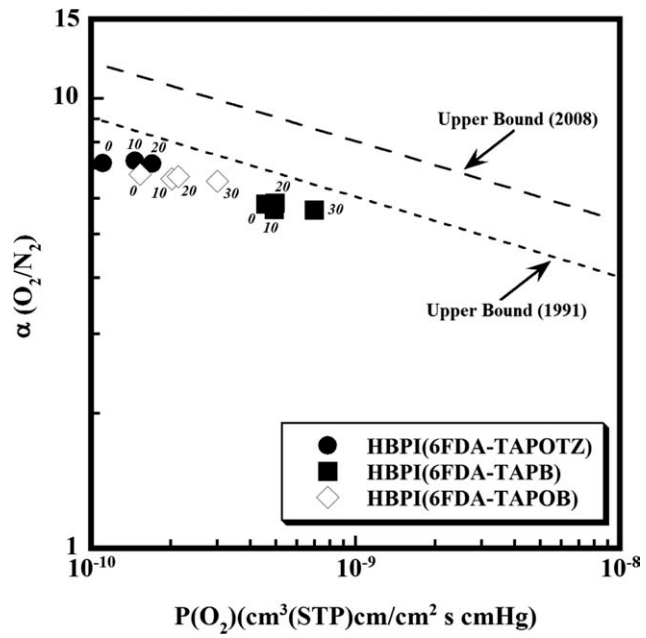

Figure 5. Ideal O_2/N_2 selectivity of HBPI–silica hybrid membranes plotted against O_2 permeability; attached number represents silica content (wt %) in the membrane.

Gas Transport Properties of HBPI–Silica Hybrid Membranes

Gas permeability, diffusion, and solubility coefficients of the hybrid membranes are summarized in Table II. Unfortunately, we could not carry out the gas permeation measurement for the HBPI(6FDA-TAPOTZ)–silica hybrid membrane containing 30 wt % of SiO_2 because of its mechanical brittleness. Gas permeability coefficients of pristine HBPI(6FDA-TAPB) are higher than those of pristine HBPI(6FDA-TAPOTZ) and HBPI(6FDA-TAPOB), attributing higher gas diffusion coefficients. It is well known that gas diffusivities of polymers strongly depend on the fractional free volumes (FFVs).[22,23] The FFVs of the pristine HBPIs calculated from eqs. (4) and (5) are listed in Table I. The HBPI(6FDA-TAPB) has the highest FFV in the three HBPIs, and the highest gas diffusivities of the HBPI(6FDA-TAPB) are, therefore, attributed to its highest FFV. Figure 4 shows CO_2 permeability, diffusion, and solubility coefficients of the hybrid membranes plotted against silica content. As shown in Figure 4

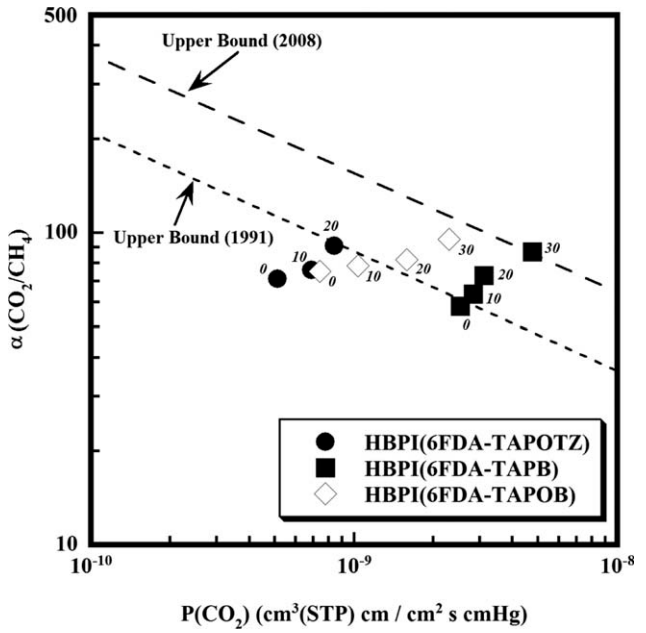

Figure 6. Ideal CO_2/CH_4 selectivity of HBPI–silica hybrid membranes plotted against CO_2 permeability; attached number represents silica content (wt %) in the membrane.

and Table II, gas permeability coefficients of the hybrid membranes increase with increasing silica content in connection with increased gas diffusion and solubility coefficients. Similar enhancements of gas permeabilities have been reported by Merkel et al. for high-free-volume, glassy polymer–nanosilica composites, and they have concluded that the nanosilica particles yield polymer/particle interfacial area and provide disruption of polymer chain packing and affect gas transport behavior.[24,25] Consequently, the increased gas permeabilities of the HBPI–silica hybrid membranes might be caused by additional formation of free volume elements around polymer/silica interfacial area, which provides diffusion path and Langmuir-type sorption site for gas molecules.[2]

The ideal gas selectivity for the combination of gases A and B (α(A/B)) is defined by the following equation;[26]

$$\alpha(A/B) = \frac{P(A)}{P(B)} = \frac{D(A)}{D(B)} \times \frac{S(A)}{S(B)} = \alpha^D(A/B) \times \alpha^S(A/B) \quad (6)$$

where $\alpha^D(A/B)$ is the diffusivity selectivity and $\alpha^S(A/B)$ is the solubility selectivity. The O_2/N_2 and CO_2/CH_4 selectivities of the hybrid membranes are summarized in Table III, and $\alpha(O_2/N_2)$ and $\alpha(CO_2/CH_4)$ values are plotted against O_2 and CO_2 permeability coefficients in Figures 5 and 6, respectively. In Figure 5, it is recognized that the $\alpha(O_2/N_2)$ values of the hybrid membranes slightly decrease with increasing O_2 permeability along with the upper bound trade-off line for O_2/N_2 separation demonstrated by Robeson in 1991.[27] This behavior is consistent with the general understanding that polymers that are more permeable are less selective, and *vice versa*.[26] In any event, it can be seen the HBPI–silica hybrid membranes have a favourable O_2/N_2 separation ability because they show high $\alpha(O_2/N_2)$ values just below the upper bound. For CO_2/CH_4 separation (Figure 6), the $\alpha(CO_2/CH_4)$ values of the hybrid membranes increase with increasing CO_2 permeability, or silica content, tending to exceed the upper bound for CO_2/CH_4 separation.[27,28] The noticeable CO_2/CH_4 separation behavior is considered to be brought by characteristic distribution and interconnectivity of free volume elements created around polymer/silica interfacial area, which provides a size-selective CO_2/CH_4 separation ability. Similarly, He et al.[29] have reported that vapour/gas separation properties of high-free-volume, glassy polymers with rigid molecular chains are improved by incorporation of nanosized inorganic fillers that disrupt molecular chain packing. It is worth noting that the HBPI(6FDA-TAPB) system possesses high CO_2/CH_4 separation ability, and especially for the hybrid membrane containing 30 wt % of SiO_2, the $\alpha(CO_2/CH_4)$ value reaches the upper bound updated in 2008. The prominent CO_2/CH_4 separation ability of the HBPI(6FDA-TAPB) system might be caused by the contributions of both intrinsic high FFV and characteristic distribution and interconnectivity of free volume elements created around polymer/silica interfacial area.

CONCLUSIONS

Physical and gas transport properties of novel HBPI–silica hybrid membranes were investigated. Glass transition and 5% weight-loss temperatures of the HBPI–silica hybrid membranes are increased with increasing silica content. The HBPI(6FDA-TAPOTZ) system, however, shows relatively low 5% weight-loss temperatures, suggesting thermal instability of triazine-ring in the TAPOTZ moiety. Gas permeability coefficients of the HBPI–silica hybrid membranes are increased with increasing silica content in connection with increased gas diffusion and solubility coefficients. This fact indicates additional formation of free volume elements around polymer/silica interfacial area, which provides diffusion path and Langmuir-type sorption site for gas molecules. CO_2/CH_4 separation ability of the HBPI–silica hybrid membranes are increased with increasing silica content, tending to exceed the upper bound for CO_2/CH_4 separation, suggesting characteristic distribution and interconnectivity of free volume elements created around polymer/silica interfacial area. Especially, the HBPI(6FDA-TAPB) system possesses high CO_2/CH_4 separation ability. The prominent CO_2/CH_4 separation ability of the HBPI(6FDA-TAPB) system might be caused by the contributions of both intrinsic high FFV and characteristic distribution and interconnectivity of free volume elements created around polymer/silica interfacial area.

REFERENCES

1. Sykes, G. F.; Clair, A. K. S. *J. Appl. Polym. Sci.* **1986,** *32*, 3725.
2. Okamoto, K.; Tanaka, K.; Kita, H.; Ishida, M.; Kakimoto, M.; Imai, Y. *Polym. J.* **1992,** *24*, 451.
3. Langsman, M.; Burgoyne, W. F. *J. Polym. Sci. Part A: Polym. Chem.* **1993,** *31*, 909.
4. Li, Y.; Wang, X.; Ding, M.; Xu, J. *J. Appl. Polym. Sci.* **1996,** *61*, 741.

5. Fang, J.; Kita, H.; Okamoto, K. *Macromolecules* **2000,** *33*, 4639.
6. Fang, J.; Kita, H.; Okamoto, K. *J. Membr. Sci.* **2001,** *182*, 245.
7. Kanehashi, S.; Sato, S.; Nagai, K. In Membrane Gas Separation; Yampolskii, Y.; Freeman, B. D., Eds.; Wiley: UK, **2010**; pp 3–27.
8. Suzuki, T.; Yamada, Y.; Tsujita, Y. *Polymer* **2004,** *45*, 7167.
9. Cornelius, C. J.; Marand, E. *J. Membr. Sci.* **2002,** *202*, 97.
10. Xiao, Y.; Low, B. T.; Hosseini, S. S.; Chung, T. S.; Paul, D. R. *Prog. Polym. Sci.* **2009,** *34*, 561.
11. Boroglu, M. S.; Gurkaynak, M. A. *Polym. Adv. Technol.* **2011,** *22*, 545.
12. Suzuki, T.; Yamada, Y. *J. Polym. Sci. Part B: Polym. Phys.* **2006,** *44*, 291.
13. Suzuki, T.; Yamada, Y.; Sakai, J.; Itahashi, K. In Membrane Gas Separation; Yampolskii, Y.; Freeman, B. D., Eds.; Wiley: UK, **2010**; pp 143–158.
14. Suzuki, T.; Yamada, Y.; Itahashi, K. *J. Appl. Polym. Sci.* **2008,** *109*, 813.
15. Takeichi, T.; Stille, J. K. *Macromolecules* **1986,** *19*, 2093.
16. Miyata, S.; Sato, S.; Nagai, K.; Nakagawa, T.; Kudo, K. *J. Appl. Polym. Sci.* **2008,** *107*, 3933.
17. van Krevelen, D. W. In Properties of Polymers; Elsevier: Amsterdam, **1990;** Chapter 4, pp 71–107.
18. Chen, H.; Yin, J. *J. Polym. Sci. Part A: Polym. Chem.* **2002,** *40*, 3804.
19. Zhu, H.; Ma, Y.; Fan, Y.; Shen, J. *Thin Solid Films* **2001,** *397*, 95.
20. Hibshman, C.; Cornelius, C. J.; Marand, E. *J. Membr. Sci.* **2003,** *211*, 25.
21. Lin, C. H. *Polymer* **2004,** *45*, 7911.
22. Park, J. Y.; Paul, D. R. *J. Membr. Sci.* **1997,** *125*, 23.
23. Thran, A.; Kroll, G.; Faupel, F. *J. Polym. Sci. Part B: Polym. Phys.* **1999,** *37*, 3344.
24. Merkel, T. C.; Freeman, B. D.; Spontak, R. J.; He, Z.; Pinnau, I.; Meakin, P.; Hill, A. J. *Science* **2002,** *296*, 519.
25. Merkel, T. C.; Toy, L. G.; Andrady, A. L.; Gracz, H.; Stejskal, E. O. *Macromolecules* **2003,** *36*, 353.
26. Freeman, B. D. *Macromolecules* **1999,** *32*, 375.
27. Robeson, L. M. *J. Membr. Sci.1991*, 62, 165.
28. Robeson, L. M. *J. Membr. Sci.* **2008,** *320*, 390.
29. He, Z.; Pinnau, I.; Morisato, A. In Advanced Materials for Membrane Separation; Pinnau, I.; Freeman, B. D., Eds.; ACS Symposium Series 876; American Chemical Society: Washington, DC, **2004**; pp 218–233.